University of Glasgow

Mao, J., Farhang, A., Zhang, L. , Chu, Z., Xiao, P. and Gu, S. (2021) Interference Analysis in Multi-Numerology OFDM Systems: A Continuous-Time Approach. In: IEEE ICC 2021-Workshops, 14-18 Jun 2021, ISBN 9781728194424 (doi:10.1109/ICCWorkshops50388.2021.9473482)

The material cannot be used for any other purpose without further permission of the publisher and is for private use only.

There may be differences between this version and the published version. You are advised to consult the publisher's version if you wish to cite from it.

http://eprints.gla.ac.uk/237870/

Deposited on 31 March 2021

Enlighten – Research publications by members of the University of Glasgow
http://eprints.gla.ac.uk

Interference Analysis in Multi-Numerology OFDM Systems: A Continuous-Time Approach

Juquan Mao[1], Arman Farhang[2], Lei Zhang[3], Zheng Chu[1], Pei Xiao[1], Sai Gu [4]
[1] Institute for Communication Systems (ICS), Home of 5G Innovation Centre, University of Surrey, Guildford, UK
[2] Department of Electronic Engineering, National University of Ireland Maynooth, Maynooth, Ireland
[3] James Watt School of Engineering, University of Glasgow, Glasgow
[4] University of Warwick, Warwick, UK
Email: juquan.mao@surrey.ac.uk

***Abstract*—Multi-numerology multi-carrier (MN-MC) techniques are considered as essential enablers for RAN slicing in fifth-generation (5G) communication systems and beyond. However, utilization of mixed numerologies breaks the orthogonality principle defined for single-numerology orthogonal frequency division multiplexing (SN-OFDM) systems with a unified subcarrier spacing. This leads to interference between different numerologies, i.e., inter-numerology interference (INI). This paper develops metrics to quantify the level of the INI using a continuous-time approach. The derived analytical expressions of INI in terms of mean square error (MSE) and error vector magnitude (EVM) directly reveal the main contributing factors to INI, which can not be shown explicitly in a matrix form INI based on discrete-time calculations. Moreover, the study of power offset between different numerologies shows a significant impact on INI, especially for high order modulation schemes. The finding in this paper provides analytical guidance in designing multi-numerology (MN) systems, for instance, developing resource allocation schemes and interference mitigation techniques.**

***Index Terms*—inter-numerology interference, mixed numerologies, MSE, OFDM, EVM**

I. Introduction

Future networks are envisioned to have the flexibility in supporting a diverse set of services and applications, e.g., autonomous driving, virtual reality and intelligent industrial systems. Wireless standards have accordingly considered the coexistence of multiple communication scenarios such as enhanced mobile broadband (eMBB), ultra-reliable and low-latency communications (URLLC), and massive machine type communications (mMTC) [1]. Each of these services has distinct quality of service (QoS) requirements, such as throughput, latency, reliability, and number of connected users to be served simultaneously. This calls for a high degree of flexibility in designing waveform parameters [2]. Conventional resource distribution adopts a single numerology[1] with uniform frame design to provide different services, as in 4G long term evolution (LTE). However, this can not provide the desired flexibility to support the services with different requirements [4]. Additionally, it is not viable to design separate radios for separate services [5].

[1]The term 'numerology' is defined as a set of parameters like subcarrier spacing, symbol length, and cyclic prefix [3]

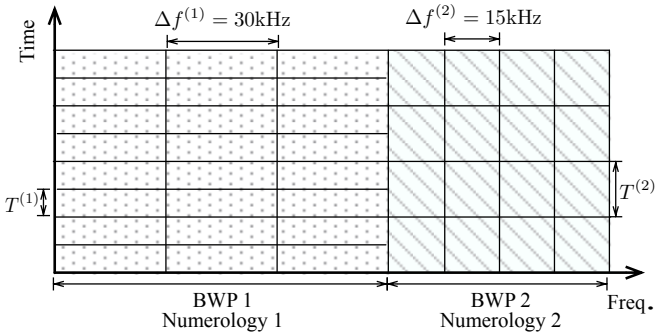

Fig. 1. Illustration of frequency and time relationship with two numerologies for the case $\nu = 2$.

In 5G new radio (NR) specifications, OFDM with mixed numerologies is considered to enable multi-service communications over a unified physical layer [6]. One viable solution is to multiplex mixed numerologies in the frequency domain, i.e., the system bandwidth is divided into several bandwidth parts (BWPs), each having a distinct numerology optimized for a particular service. As an example shown in Fig. 1, two different numerologies associated with 15 kHz and 30 kHz subcarrier spacings are mixed. It is worth noting that these values for subcarrier spacing are inline with 5G NR specifications where the wider subcarrier spacing can be utilized for applications with URLLC requirement such as autonomous driving. However, coexistence of mixed numerologies makes the time-frequency lattice irregular and hence causes inter-numerology interference (INI) because subcarriers associated with differing numerologies will no longer be orthogonal to one other [7]. This complicates both signal generation and detection in multi-numerology orthogonal frequency division multiplexing (MN-OFDM) systems.

Consequently, it is of a paramount importance to understand INI effects in OFDM with multiple numerologies. To this end, in [8], the authors developed a generic framework for fast convolution-based f-OFDM (FC-f-OFDM) waveform with multiple numerologies and provided INI. In [9], the authors introduced a framework for MN subband filtered multi-carrier (SFMC) systems where the INI was analyzed in presence of

transceiver imperfections and insufficient guard interval between the symbols. The authors in [10] derived expressions for the INI of MN windowed OFDM and used the expressions as the basis for development of a novel interference cancellation scheme. The authors in [11] established an analytical system model to explore OFDM and f-OFDM. This analytical system model was also deployed in designing a power allocation scheme that maximizes the sum-rate. In a more recent work, the authors in [12] investigated a MN non-orthogonal multiple access (MN-NOMA) scheme where the analytical expressions for the INI experienced by each user at the receiver were derived.

All the above-mentioned studies derive matrix form INI expressions based on a finite sum of discrete samples of complex exponential functions. We refer to such derivations as sum-of-exponentials (SoE) form. A major disadvantage of such a approach is that the main contributing factors to INI are concealed. Our previous work in [13] solved the issue by deriving reduced-form interference formulas. This simplifies the expression into a pulse-shape function sinc(d), where d represents the relative distance between the two MN subcarriers. The reduced-form expressions explicitly reveal that the pulse shape function, the relative distance, and the numerology scaling factor are the primary contributors to INI effects. This paper generalizes the INI derivations for only two MN subcarriers in [13] to the total INI that any given data symbol suffers from all the others. To further study and quantify INI effects, we also analytically derive the metrics such as mean square error (MSE) and error vector magnitude (EVM) of the received symbols. Such work is important as our MSE and EVM derivations can be used to develop efficient resource allocation schemes and/or advanced parameter adjustment schemes for MN-OFDM systems. Moreover, the impact of power offset factor between two numerologies to the interference is also studied.

The rest of this paper is organized as follows. Section II presents the MN-OFDM system model. In Section III, we derive the analytical expression of the total interference and develop MSE and EVM of the received data symbols as metrics to quantify the INI level. In SectionIV, we assess the validity of our derivations through numerical results. Finally, the paper is concluded in Section V.

Notations: boldface lower-case characters are used to denote vectors, $(\cdot)^*$ denotes complex conjugate operation, $\mathbb{R}$ and $\mathbb{Z}$ represent the set of all real numbers and integers, respectively. $\mathbb{E}[\cdot]$ denotes the expectation operator, and the superscript $(\cdot)^{(i)}$ is used to denote numerology i.

II. System Model

To purely study the effect of interference from one numerology to another, without loss of generality, in our system model, we consider two differing numerologies[2], namely, numerology 1 and numerology 2. The subcarrier spacing $\Delta f^{(i)}$ and symbol duration $T^{(i)}$ associated with different numerologies i, $i = \{1, 2\}$, are related to one another via a scaling factor ν, where

$$\frac{\Delta f^{(1)}}{\Delta f^{(2)}} = \frac{T^{(2)}}{T^{(1)}} = \nu. \tag{1}$$

Assuming $\Delta f^{(1)} > \Delta f^{(2)}$ with the scaling factor being greater than 1, and based on 5G NR specifications [6], ν is only chosen as powers of two, $\nu = 2^{\mu}, \mu \in \{1, 2, \cdots\}$. Fig. 1 represents the time-frequency relation with two numerologies for $\nu = 2$ where $\Delta f^{(1)} = 2\Delta f^{(2)}$ and $\Delta T^{(1)} = 0.5\Delta T^{(2)}$. As it is shown in this figure, each symbol associated with numerology 2 overlaps with two symbols associated with numerology 1 in the time domain.

Fig. 2 depicts the block diagram of a continuous-time MN-OFDM baseband model[3], where the MN-OFDM modulator/demodulator consists of two SN-OFDM modulators/demodulators associated with the two numerologies, respectively. In this setup, the system bandwidth is divided into two non-overlapped BWPs associated with the two numerologies. It is worth mentioning that we consider different numerologies for different BWPs. Thus, in the rest of the paper, the terms "BWP" and "numerology" are used interchangeably.

We consider arranging the system bit stream in a block vector $\mathbf{b}$, and the bit stream for numerology i in a block vector $\mathbf{b}^{(i)}$. The bit stream $\mathbf{b}$ is divided into two substreams via a BWP mapper. The i-th substream $\mathbf{b}^{(i)}$ associated with BWP i, and occupying bandwidth $B^{(i)}$, $i = \{1, 2\}$, is linearly modulated, typically using quadrature amplitude modulation (QAM) or phase-shift keying (PSK). We assume coherent demodulation of the subcarriers so that the subcarrier phase is neglected in our analysis. After serial-to-parallel conversion, a group of complex symbols $\mathbf{s}^{(i)}$ is modulated via a SN-OFDM modulator for each numerology. The signal $x^{(i)}(t)$ associated with a given numerology i at symbol k can be written as

$$x_k^{(i)}(t) = \sum_{m \in \mathcal{N}_{\text{act}}^{(i)}} s_{k,m}^{(i)} \phi_m^{(i)}(t - kT^{(i)}), \tag{2}$$

where $\mathcal{N}_{\text{act}}^{(i)}$ is the set of all the active subcarriers associated with numerology i. The complex symbol $s_{k,m}^{(i)}$ is the one to be transmitted in the time window $[kT^{(i)}, (k+1)T^{(i)}]$, $k \in \mathbb{Z}$, over the m-th active subcarrier centered at the frequency $f_m^{(i)} = m\Delta f^{(i)}$. The normalized, frequency-shifted rectangular pulse $\phi_m^{(i)}(t)$ is defines as

$$\phi_m^{(i)}(t) = \begin{cases} \frac{1}{\sqrt{T^{(i)}}} \exp(j2\pi \frac{m}{T^{(i)}} t) & 0 \le t \le T^{(i)} \\ 0 & \text{otherwise} \end{cases}. \tag{3}$$

The transmit signal $x(t)$ is then obtained by multiplexing the truncated/concatenated single-numerology signals associated with both the numerologies. Ignoring the additive noise, the mixed signal at the receiver takes different forms for numerology 1 and 2 with respect to the symbol duration. Therefore, the signal $x(t)$ in the time window corresponding to symbol

[2]Research findings gained in this paper can be easily extend to any number of numerologies.

[3]Although a discrete-time model is more efficient to implement, a continuous-time model allows an easy understanding of the principles.

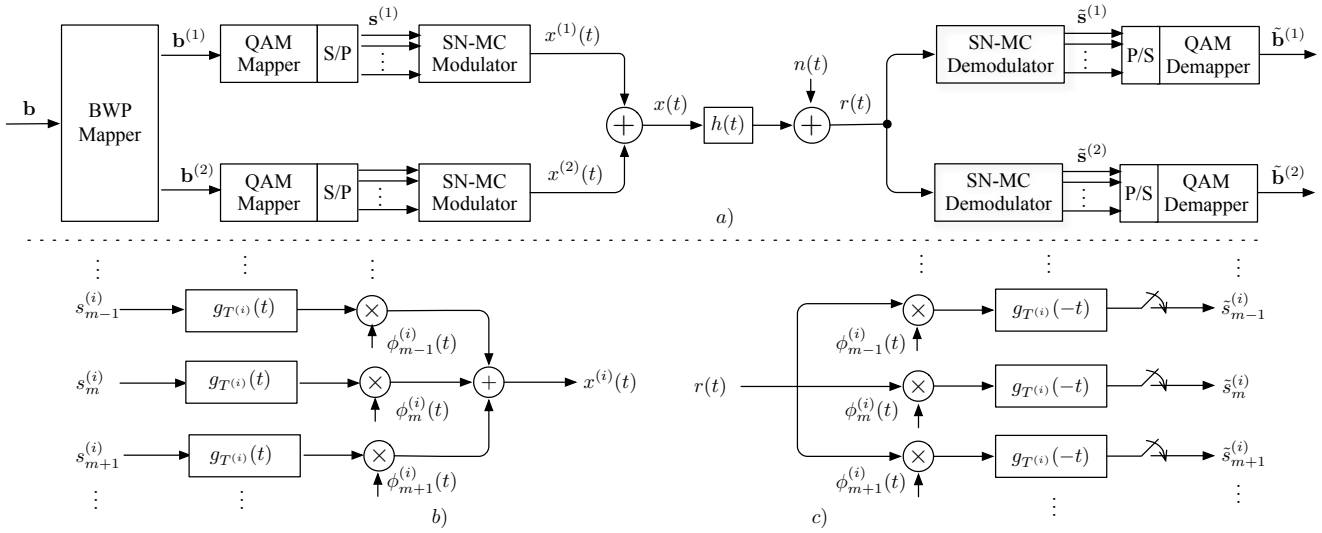

Fig. 2. A signal model with two numerologies. a) Multi-numerology OFDM modulator. b) Multi-numerology OFDM demodulator.

k for numerology 1 can be expressed as

$$x_k(t) = x_k^{(1)}(t) + x^{(2)}_{\lfloor \frac{k}{v} \rfloor}(t),\ t \in [kT^{(1)}, (k+1)T^{(1)}], \quad (4)$$

where $\lfloor \cdot \rfloor$ is the floor function. The signal $x(t)$ in the time window for symbol k of numerology 2, can be written as

$$x_k(t) = \sum_{q=0}^{\nu-1} x^{(1)}_{\nu k+q} + x_k^{(2)}(t),\ t \in [kT^{(2)}, (k+1)T^{(2)}]. \quad (5)$$

Equations (4) and (5) mathematically describe what Fig. 1 illustrates, i.e, how signals of different symbol duration overlap in the time domain. In particular, the k-th symbol associated with numerology 1 overlaps with a truncated portion of the $\lfloor \frac{k}{\nu} \rfloor$-th symbol associated with numerology 2, and the kth symbol associated with numerology 2 coincides with a block of ν consecutive symbols starting from the (νk)-th symbol associated with numerology 1.

As shown in Fig. 2, the received signal is passed through SN-OFDM demodulators in order to separate signals on different subcarriers within each numerology and reject signals from the other numerology. To solely study the effect of INI, in this paper, we focus on investigating the intrinsic interference caused by the MN-OFDM modulator/demodulator only, while the extrinsic wireless environments such as the channel $h(t)$ and noise $n(t)$ shall be ignored. Thus, the received signal $r(t) = x(t)$. The recovered complex symbol transmitted within the time window $[kT^{(i)}, (k+1)T^{(i)}]$ over the m-th subcarrier associated with numerology i can be obtained as

$$\tilde{s}^{(i)}_{k,m} = \int_{kT^{(i)}}^{(k+1)T^{(i)}} r_k(t) \phi_m^{(i)*}(t - kT^{(i)})\ dt. \quad (6)$$

The demodulated symbols are then combined using a parallel-to-serial converter and a symbol-to-bit demapper to form the original bit stream for each numerology.

III. Quantifying the INI in multi-numerology systems

Data symbols that are modulated onto two subcarriers interfere with one another when the inner product of the two subcarriers is not equal to zero. The magnitude of the inner product exhibits the correlation between two subcarriers. In particular, the greater the magnitude of the inner product, the higher the correlation between the two subcarriers and hence a larger amount of interference. Therefore, the magnitude of the inner product can be leveraged to measure the interference level. In this section, we first derive the expression of the interference from a symbol to another one associated with a different numerology, then we develop metrics for the total interference to a symbol from the added signal of another numerology.

A. INI from one symbol to another with different numerologies

Substituting (4) into (6) yields the received symbol on subcarrier m associated with numerology 1 as

$$\tilde{s}^{(1)}_{m,k} = \int_{kT^{(1)}}^{(k+1)T^{(1)}} \left(x_k^{(1)}(t) + x^{(2)}_{\lfloor \frac{k}{v} \rfloor}(t) \right) \phi_m^{(1)*}(t - kT^{(1)}) dt. \quad (7)$$

Substituting (2) into (7), we have

$$\tilde{s}^{(1)}_{m,k} = \sum_{n \in \mathcal{N}^{(1)}_{\text{act}}} s^{(1)}_{k,n} \int_{kT^{(1)}}^{(k+1)T^{(1)}} \phi_n^{(1)}(t - kT^{(1)}) \phi_m^{(1)*}(t - kT^{(1)}) dt + \sum_{n \in \mathcal{N}^{(2)}_{\text{act}}} s^{(2)}_{\lfloor \frac{k}{v} \rfloor, n} \int_{kT^{(1)}}^{(k+1)T^{(1)}} \phi_n^{(2)}(t - \lfloor \frac{k}{\nu} \rfloor T^{(2)}) \phi_m^{(1)*}(t - kT^{(1)}) dt. \quad (8)$$

With the change of variable $u = t - kT^{(1)}$, (8) reduces to

$$\tilde{s}^{(1)}_{m,k} = \sum_{n \in \mathcal{N}^{(1)}_{\text{act}}} s^{(1)}_{k,n} \int_0^{T^{(1)}} \phi_m^{(1)*}(u) \phi_n^{(1)}(u) du + \sum_{n \in \mathcal{N}^{(2)}_{\text{act}}} s^{(2)}_{\lfloor \frac{k}{v} \rfloor, n} \exp(j\theta_{n,k}) \int_0^{T^{(1)}} \phi_m^{(1)*}(u) \phi_n^{(2)}(u) du, \quad (9)$$

where the phase shift $\theta_{n,k} = 2\pi kn/\nu$. The second term in (9) follows the derivation

$$\begin{aligned}\phi_n^{(2)}(t - \lfloor\frac{k}{\nu}\rfloor T^{(2)}) &= \phi_n^{(2)}(u + kT^{(1)} - \lfloor\frac{k}{\nu}\rfloor T^{(2)}) \\ &\overset{(a)}{=} \sqrt{T^{(2)}}\phi_n^{(2)}(kT^{(1)} - \lfloor\frac{k}{\nu}\rfloor T^{(2)})\phi_n^{(2)}(u) \\ &= \exp(j2\pi n\frac{k}{\nu})\exp(-j2\pi n\lfloor\frac{k}{\nu}\rfloor)\phi_n^{(2)}(u) \\ &\overset{(b)}{=} \exp(2j\pi n\frac{k}{\nu})\phi_n^{(2)}(u), \end{aligned} \tag{10}$$

where equality (a) follows (3) and equality (b) is due to the fact that $\lfloor\frac{k}{\nu}\rfloor \in \mathbb{Z}$, and thus, $\exp(-2j\pi n\lfloor\frac{k}{\nu}\rfloor) = 1$.

According to the reduced-form formulas for the inner product of subcarriers in [13], we have

$$\begin{aligned}&\int_0^{T^{(1)}} \phi_m^{(1)^*}(u)\phi_n^{(1)}(u)du = \delta(m-n) \\ &\int_0^{T^{(1)}} \phi_m^{(1)^*}(u)\phi_n^{(2)}(u)du = \sqrt{\frac{1}{\nu}}\exp(-j\pi d_{m,n}^{(1\leftarrow 2)})\mathrm{sinc}(d_{m,n}^{(1\leftarrow 2)}) \end{aligned} \tag{11}$$

where $\delta(x)$ denotes Dirac function which is 1 for $x = 0$ and 0 otherwise, and $d_{m,n}^{(1\leftarrow 2)}$ refers to the relative distance between subcarrier m associated with numerology 1 and subcarrier n associated with numerology 2. It is expressed as

$$d_{m,n}^{(1\leftarrow 2)} = \frac{m\Delta f^{(1)} - n\Delta f^{(2)}}{\Delta f^{(1)}} = m - \frac{n}{\nu}, \tag{12}$$

which is the actual distance between the two subcarriers normalized by $\Delta f^{(1)}$.

Substituting (11) into (9), yields

$$\begin{aligned}\tilde{s}_{m,k}^{(1)} &= \sum_{n\in\mathcal{N}_{\text{act}}^{(1)}} s_{k,n}^{(1)}\delta(m-n) \\ &\quad + \sum_{n\in\mathcal{N}_{\text{act}}^{(2)}} \frac{\exp(j\tilde{\theta}_{n,k})\mathrm{sinc}(d_{m,n}^{(1\leftarrow 2)})}{\sqrt{\nu}} s_{\lfloor\frac{k}{v}\rfloor,n}^{(2)} \\ &= s_{m,k}^{(1)} + \sum_{n\in\mathcal{N}_{\text{act}}^{(2)}} \mathrm{I}_{k,m,n}^{(1\leftarrow 2)}, \end{aligned} \tag{13}$$

where the phase shift $\tilde{\theta}_{n,k} = 2\pi kn/\nu - \pi d_{m,n}^{(1\leftarrow 2)}$, the interference term $\mathrm{I}_{k,m,n}^{(1\leftarrow 2)}$ refers to the INI from a smaller numerology to a larger one, and it is expressed as

$$\mathrm{I}_{k,m,n}^{(1\leftarrow 2)} = \frac{\exp(j\tilde{\theta}_{n,k})\mathrm{sinc}(d_{m,n}^{(1\leftarrow 2)})}{\sqrt{\nu}} s_{\lfloor\frac{k}{v}\rfloor,n}^{(2)}, \tag{14}$$

where $s_{\lfloor\frac{k}{v}\rfloor,n}^{(2)}$ is the transmit symbol of numerology 2 which concurrents with symbol $s_{m,k}^{(1)}$.

Subsequently, substituting (4) and (2) into (6), following the same line of derivations as above for the received symbol associated with numerology 1, we can express the received symbol on subcarrier m associated with numerology 2 as

$$\begin{aligned}\tilde{s}_{m,k}^{(2)} &= \sum_{n\in\mathcal{N}_{\text{act}}^{(2)}} s_{k,n}^{(2)}\delta(m-n) \\ &\quad + \sum_{n\in\mathcal{N}_{\text{act}}^{(1)}} \sum_{q=0}^{\nu-1} s_{\nu k+q}^{(1)} \int_0^{T^{(1)}} \phi_m^{(2)^*}(t)\phi_n^{(1)}(t)dt \\ &= s_{m,k}^{(2)} + \sum_{n\in\mathcal{N}_{\text{act}}^{(1)}} \mathrm{I}_{k,m,n}^{(2\leftarrow 1)}, \end{aligned} \tag{15}$$

TABLE I
COMPLEXITY FOR CALCULATING $\mathrm{I}_{k,m,n}^{(1\leftarrow 2)}$

Operation	Existing studies [8]–[11]	This work
$+/-$	$N^{(1)}$	2
$\times/\div$	$18N^{(1)}$+1	8
$\sqrt{\cdot}$	N/A	1
$\exp(\cdot)$	$2N^{(1)}$	1
$\mathrm{sinc}(\cdot)$	N/A	1

where $\mathrm{I}_{k,m,n}^{(2\leftarrow 1)}$ represents the INI from a larger numerology to a smaller one, which is expressed as

$$\mathrm{I}_{k,m,n}^{(2\leftarrow 1)} = \sum_{q=0}^{\nu-1} \frac{\exp(j\pi d)\mathrm{sinc}(d_{m,n}^{(1\leftarrow 2)})}{\sqrt{\nu}} s_{\nu k+q,n}^{(1)} \tag{16}$$

where the symbols $s_{k\nu+q,n}^{(1)}, q = 0, 1, \cdots, \nu-1$ are interfering with the symbol $s_{m,k}^{(2)}$.

It can be seen that (14) and (16) establish relationship between INI and the rectangular pulse-shape function (sinc), i.e., the magnitude of INI is proportional to magnitude of sinc. The reduced-form formulas in (14) and (16) lead to a significantly reduced complexity of calculating INI in comparison with the SoE forms of the existing studies [8]–[11]. As an example, Table I compares the complexity for calculating $\mathrm{I}_{k,m,n}^{(1\leftarrow 2)}$ between the existing studies and this work, where the complexity is shown in terms of the number of basic operations listed in the table. Based on the table, the complexity using our proposed method is reduced by at least $N^{(i)}$ times, where $N^{(i)} = B/\Delta f^{(i)}$ with B being the system bandwidth. This amount of saving in complexity is of a paramount importance for applications that require interference calculations, such as resource scheduling based on signal quality.

B. Total INI to a symbol from the added signal of another numerology

Taking into account of all the symbols on the active subcarriers associated with the interfering numerology o, we can quantify the total instantaneous INI to the interfered symbol $s_{k,m}^{(i)}$ in terms of MSE. Assuming data symbols are independent, identically distributed zero mean random variables with the variance $(\sigma_s^{(i)})^2$, $\mathbb{E}\left[s_{k,m}^{(i)}(s_{k,m}^{(i)})^*\right] = (\sigma_s^{(i)})^2$, the MSE of the symbol on subcarrier m associated with numerology i can be obtained as

$$\mathrm{MSE}_m^{(i\leftarrow o)} = \frac{\mathbb{E}\left[\left|s_{k,m}^{(i)} - \tilde{s}_{k,m}^{(i)}\right|^2\right]}{\mathbb{E}\left[s_{k,m}^{(i)}(s_{k,m}^{(i)})^*\right]} = \frac{\mathbb{E}\left[\left|s_{k,m}^{(i)} - \tilde{s}_{k,m}^{(i)}\right|^2\right]}{(\sigma_s^{(i)})^2} \quad i, o \in \{1,2\}, i \neq o. \tag{17}$$

According to (13) and (15), (17) can be rewritten as

$$\mathrm{MSE}_m^{(i\leftarrow o)} = \sum_{n\in\mathcal{N}_{\text{act}}^{(o)}} \frac{\mathbb{E}\left[\left|\mathrm{I}_{k,m,n}^{(i\leftarrow o)}\right|^2\right]}{(\sigma_s^{(i)})^2}. \tag{18}$$

Substituting (13) into (18), we obtain

$$\mathrm{MSE}_m^{(1\leftarrow 2)} = \sum_{n\in\mathcal{N}_{\mathrm{act}}^{(2)}} \frac{\mathbb{E}\left[\left|\mathrm{I}_{k,m,n}^{(1\leftarrow 2)}\right|^2\right]}{(\sigma_s^{(1)})^2}$$
$$= \sum_{n\in\mathcal{N}_{\mathrm{act}}^{(2)}} \frac{\zeta^{(1\leftarrow 2)}}{\nu}\left|\mathrm{sinc}\left(d_{m,n}^{(1\leftarrow 2)}\right)\right|^2, \quad (19)$$

where $\zeta^{(1\leftarrow 2)} = (\sigma_s^{(2)})^2/(\sigma_s^{(1)})^2$ is the power offset factor between the numerology 2 and 1. The numerology scaling factor ν in denominator indicates that only a portion of power of each symbol associated with numerology 2 contributes to the interference of a symbol associated with numerology 1. This is due to the fact that symbol length of numerology 2 is ν times longer that its peer.

Substituting (15) into (18), and following the same procedure in (19), we obtain the MSE of the received signal on the subcarrier m associated with numerology 2 as

$$\mathrm{MSE}_m^{(2\leftarrow 1)} = \sum_{n\in\mathcal{N}_{\mathrm{act}}^{(1)}}\sum_{q=0}^{\nu-1} \frac{\zeta^{(2\leftarrow 1)}}{\nu}\left|\mathrm{sinc}\left(d_{m,n}^{(1\leftarrow 2)}\right)\right|^2$$
$$= \sum_{n\in\mathcal{N}_{\mathrm{act}}^{(1)}} \zeta^{(2\leftarrow 1)}\left|\mathrm{sinc}\left(d_{m,n}^{(1\leftarrow 2)}\right)\right|^2. \quad (20)$$

where $\zeta^{(2\leftarrow 1)} = (\sigma_s^{(1)})^2/(\sigma_s^{(2)})^2$ is the power offset factor between numerology 1 and 2. The numerology factor ν in (20) shows that each symbol in numerology 2 is interfered by ν overlapping symbols from numerology 1.

The worst-case MSE is defined as the upper bound MSE value over all active subcarriers of a numerology, which can be expressed as

$$\mathrm{MSE}_{\max}^{(i\leftarrow o)} = \max_{m\in\mathcal{N}_{\mathrm{act}}^{(i)}} \mathrm{MSE}_m^{(i\leftarrow o)}, \quad i,o\in\{1,2\}. \quad (21)$$

The error vector magnitude (EVM) is defined as the square root of the MSE values averaged over all active subcarriers, expressed as

$$\mathrm{EVM}^{(i\leftarrow o)} = \sqrt{\frac{\sum_{m\in\mathcal{N}_{\mathrm{act}}^{(i)}}\left|\mathrm{MSE}_m^{(i\leftarrow o)}\right|^2}{\mathrm{card}(\mathcal{N}_{\mathrm{act}}^{(i)})}}, \quad i,o\in\{1,2\}, \quad (22)$$

where $\mathrm{card}(\mathcal{N}_{\mathrm{act}}^{(i)})$ represents the number of active subcarriers associated with numerology i.

The INI expressions in (14), (16) and MSE expression in (19), (20) reveal the influencing factors to the INIs in a very explicit way, and the sinc functions play a critical part in defining the behaviour of the INI. It can be seen that the INIs decay slowly with the relative distance $d_{m,n}^{(1\leftarrow 2)}$ defined in (12) with the subcarrier indices m, n, and numerology scaling factor ν. The sinc functions inherently come from the rectangular pulse which could be replaced by better-localized pulses that decay more rapidly. This suggests that spectrum confinement techniques such as filtering and windowing which offers a better localized spectrum, can be exploited in MN-OFDM systems as an approach to mitigate INI. The relative distance can be adjusted by placing number of guard carriers between two numerologies, and more guard carriers mean greater distance, thus, less interference. Following that the numerology scaling factors $\nu > 1$, (14), (16) and (19), (20) also show that, for the two interfering symbols of the same power, the symbol modulated on the subcarrier with a smaller subcarrier spacing suffers more interference than the other.

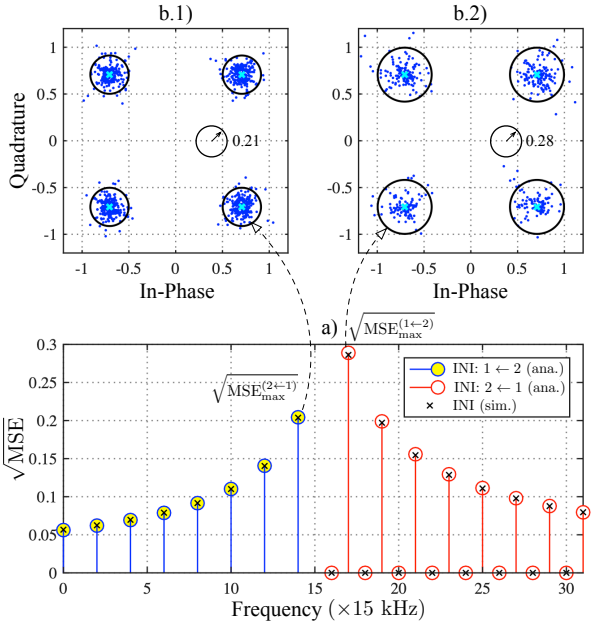

Fig. 3. MSE and modulation errors for 4-QAM with two numerologies. Parameters of numerology 1: subcarrier spacing $\Delta f^{(1)} = 30$ kHZ, the set of active subcarriers $\mathcal{N}_{\mathrm{act}}^{(1)} = \{0, 1, \cdots, 7\}$. Parameters of numerology 2: $\Delta f^{(2)} = 15$ kHZ, $\mathcal{N}_{\mathrm{act}}^{(2)} = \{16, 17, \cdots, 31\}$. a) $\sqrt{\mathrm{MSE}}$ vs. subcarrier frequency. b.1) Constellation of received symbols associated with numerology 1. b.2) Constellation of received symbols associated with numerology 2.

IV. Numerical Results

The worst-case MSE in (21) and EVM in (22) can be used to measure the modulation errors in symbol constellations, while the former reflects the worst-case error, the latter measures the average error. Figures 3 and 4 illustrate the INI between two numerologies in terms of MSE/EVM and the impact on the modulation errors caused by the interference. The simulation parameters used to obtain the results are given in the caption under the Fig.3. It is worth mentioning that INI mitigation techniques are generally out of the scope of this paper, and the numerical/analytical results may represent the worst cases without any INI mitigation methods employed.

Fig 3 a) depicts the square root of MSE versus subcarrier frequency. It can be seen that the subcarriers on the edges of the band for each numerology suffer more than other subcarriers that are relatively distant from interfering subcarriers. As it is shown in the figure, the worst-case MSE for numerology 1 occurs on the last active subcarrier, and the worst-case MSE for numerology 2 happens on the first active subcarrier. It can also be seen that the MSE for numerology 2 is generally larger than numerology 1. This suggests that smaller numerologies

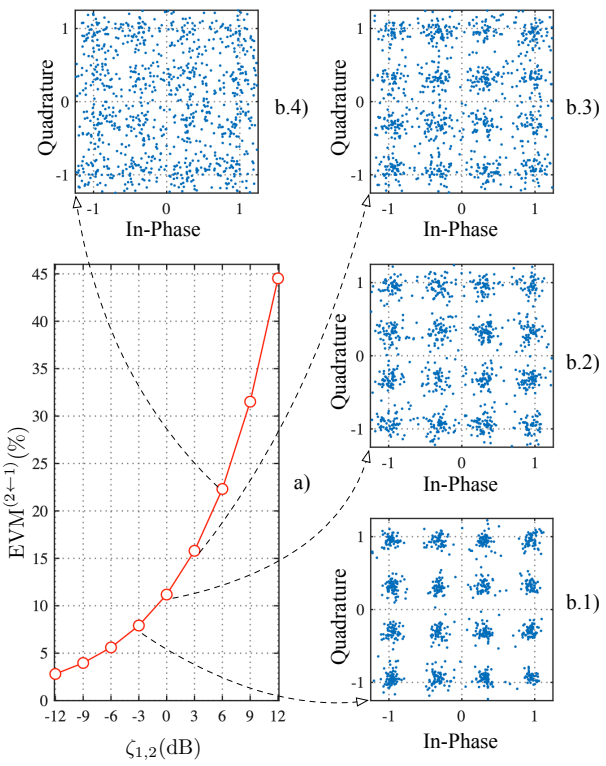

Fig. 4. EVM and modulation errors for 16-QAM with two numerologies (same parameters as specified in Fig. 3). a) EVM for numerology 2 vs mean power ratio $\zeta^{(2\leftarrow1)}$ between numerology 1 and numerology 2. b.1) - b.4) Constellations of received symbols associated with numerology 1 with $\zeta^{(2\leftarrow1)}$ = -3 dB, 0 dB, 3 dB, and 6dB, respectively.

are subject to a higher amount of INI than larger ones. This is further confirmed by the other two subfigures: Fig 3 b.1) and b.2), where the constellations for received symbols are provided for numerology 1 and 2, respectively. The radius of the circles measured by square root of the worst-case MSEs indicates the quality of received symbols.

We demonstrate the impact of the power offset factors on the INI in Fig. 4. From this figure, it can be seen that the EVM for numerology 2 increases as the power offset factor $\zeta^{(2\leftarrow1)}$ grows. The corresponding constellations for $\zeta^{(2\leftarrow1)}$ = -3dB, 0dB, 3dB, 6dB are given in subfigures b.1) to b.4). It shows that, when $\zeta^{(2\leftarrow1)}$ reaches 6dB, it becomes extremely hard to identify the decision boundaries among different constellation points for 16-QAM. It is expected to be even worse for high order modulation schemes like 64-QAM, 256-QAM, etc. This signifies the importance of INI mitigating techniques to ensure a good quality of received symbols in presence of power imbalance between different numerologies, especially for high-order modulation schemes.

V. Conclusions

In this paper, we studied INI caused by the coexistence of mixed numerologies in MN-OFDM systems. We first derived the expression of the total interference that a data symbol suffers from all other overlapped symbols in the time domain. Based on the derived analytical expressions, the metrics to quantify the level of INI with respect to MSE and EVM were calculated, which fundamentally defines the maximum signal-to-interference ratio (SIR) that can be achieved at the receiver, if there are no other impairments to the signal between transmitter and receiver. Moreover, the power offset between differing numerologies is shown to have a significant impact on INI, especially for high-order modulation schemes. This paper highlighted the measurement of the INI with regard to the modulation error due to the coexistence of mixed numerologies; therefore, the design of the MN-OFDM systems can exploit the developed metrics to quantify the transmitted signal quality and validates whether the transmitted signal meets defined minimum signal quality requirements. The work presented in this paper also provides scope for future research, such as deriving INI in presence of channels, developing resource allocation schemes and interference mitigation techniques in MN-OFDM systems.

References

[1] M. Series, "IMT Vision–Framework and Overall Objectives of the Future Development of IMT for 2020 and Beyond," *Recommendation ITU*, 2015.

[2] B. Yang, L. Zhang, O. Onireti, P. Xiao, M. A. Imran, and R. Tafazolli, "Mixed-Numerology Signals Transmission and Interference Cancellation for Radio Access Network Slicing," *IEEE Trans. Wireless Commun.*, pp. 1–14, 2020.

[3] A. A. Zaidi, R. Baldemair, H. Tullberg *et al.*, "Waveform and Numerology to Support 5G Services and Requirements," *IEEE Commun. Mag.*, vol. 54, no. 11, pp. 90–98, 2016.

[4] P. Banelli, S. Buzzi, G. Colavolpe *et al.*, "Modulation Formats and Waveforms for 5G Networks: Who Will be the Heir of OFDM?: An Overview of Alternative Modulation Schemes for Improved Spectral Efficiency," *IEEE Signal Process. Mag.*, vol. 31, no. 6, pp. 80–93, 2014.

[5] L. Zhang, A. Ijaz, P. Xiao, and R. Tafazolli, "Multi-Service System: An Enabler of Flexible 5G Air Interface," *IEEE Commun. Mag*, vol. 55, no. 10, pp. 152–159, 2017.

[6] 3GPP, "NR; Physical Channels and Modulation," 3rd Generation Partnership Project, TS 38.211, 09 2018.

[7] A. Yazar and H. Arslan, "A Flexibility Metric and Optimization Methods for Mixed Numerologies in 5G and Beyond," *IEEE Access*, vol. 6, pp. 3755–3764, 2018.

[8] J. Yli-Kaakinen, T. Levanen, S. Valkonen, K. Pajukoski, J. Pirskanen, M. Renfors, and M. Valkama, "Efficient Fast-Convolution-Based Waveform Processing for 5G Physical Layer," *IEEE J. Select. Areas Commun.*, vol. 35, no. 6, pp. 1309–1326, 2017.

[9] L. Zhang, A. Ijaz, P. Xiao *et al.*, "Subband Filtered Multi-Carrier Systems for Multi-Service Wireless Communications," *IEEE Trans. Wireless Commun.*, vol. 16, no. 3, pp. 1893–1907, 2017.

[10] X. Zhang, L. Zhang, P. Xiao *et al.*, "Mixed Numerologies Interference Analysis and Inter-Numerology Interference Cancellation for Windowed OFDM Systems," *IEEE Trans. Veh. Technol.*, 2018.

[11] J. Mao, L. Zhang, P. Xiao, and K. Nikitopoulos, "Interference Analysis and Power Allocation in the Presence of Mixed Numerologies," *IEEE Trans. Wireless Commun.*, 2020.

[12] S. McWade, M. F. Flanagan, L. Zhang, and A. Farhang, "Interference and Rate Analysis of Multinumerology NOMA," *arXiv preprint arXiv:2002.11588*, 2020.

[13] J. Mao, L. Zhang, S. McWade, H. Chen, and P. Xiao, "Characterizing Inter-Numerology Interference in Mixed-Numerology OFDM Systems," *arXiv preprint arXiv:2009.13348*, 2020.